ACS Photonics

Article

pubs.acs.org/journal/apchd5

Enhanced Second Harmonic Generation by Coupling to Exciton Ensembles in Ag-coated ZnO Nanorods

Jerome K. Hyun,[†] Taehee Kang,[‡] Hyeonjun Baek,[‡] Hongseok Oh,[‡] Dai-sik Kim,[‡] and Gyu-chul Yi*[,‡]

[†]Department of Chemistry and Nano Science, Ewha Womans University, Seoul 120-750, Republic of Korea

[‡]Department of Physics and Astronomy, Seoul National University, Seoul 151-742, Republic of Korea

Supporting Information

ABSTRACT: We report UV emission from a ZnO nanorod (NR) highly enhanced by coupling of excitons to cavity-enhanced second harmonic generation (SHG). A Ag cavity concentrates the exciting field into the center of the NR, producing an enhanced second harmonic (SH) response through the nonlinearity of ZnO, that spatially overlaps with an ensemble of excitons. Strong coupling to the excitons at room temperature is achieved when the SH response is spectrally tuned to the exciton transition through the NR diameter, yielding total SHG enhancements of 2 orders of magnitude. Our approach highlights a unique and simple platform for enhancing coherent, nonlinear light−matter interactions in a size regime that is challenging for plasmonic architectures, yet important for optoelectronics.

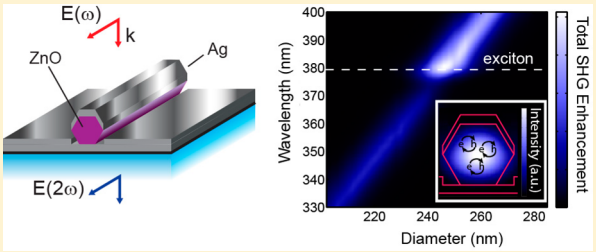

KEYWORDS: *exciton−photon coupling, second harmonic generation, nanowire, nanorod, light−matter interaction, metal−semiconductor hybrids*

Strategies for raising the optical nonlinearities of materials are an active research theme with rich and broad implications in integrated plasmonics,[1] subwavelength biological imaging,[2] information storage, and optical computing. In particular, nanoscale integration schemes with metallic architectures have proven popular for enhancing both linear[3−6] and nonlinear[7−9] optical properties through heightened light−matter interactions and have been demonstrated in multiple configurations,[8] including metallic nanoparticles (NP) or cavities coupled to nanowires (NWs) or nanorods (NRs). Often times the plasmonic near-field is exploited to enhance the photoluminescence (PL),[10] Raman,[11] and photocurrents[12] of small-diameter NWs (<160 nm), where the strong plasmonic near-field extends into the bulk of the NW. One challenge that arises from such systems is the emergence of surface contributions to the overall response. In order to avoid surface effects, larger NWs or NRs (>200 nm) can be used for larger bulk contributions, but a different strategy is necessary for the photons to access the NW center because the plasmonic near-field is evanescent. Such sizes also constitute a practical regime for optoelectronics,[13] furthering their importance. One solution is to enhance the fundamental Mie resonance with a metallic shell using light polarized parallel to the NW axis. In this case, the field can be concentrated deep into the center of the NW, enabling large spatial overlap between photons and bulk states that are spatially removed from the metallic interface.

An important prerequisite for realizing strong light−matter interactions in the nonlinear regime is establishing spectral overlap between the nonlinear light and optical transitions. To address this issue, we enhanced the Mie resonance of a ZnO NR in the fundamental harmonic (FH) through a Ag-cavity, and tuned its SH response to coincide spectrally and spatially with the free excitons (FX) of ZnO. Several studies of enhanced SHG in nanostructures,[7,14] including a recent one with a similar structure,[15] have demonstrated enhancements originating from increased fundamental fields, but have not addressed enhancements from coupling of SHG to bulk transitions. Our approach provides the unique opportunity to investigate nonlinear light−matter interactions in the form of SHG and ensures that coherence is maintained by satisfying the phase-matching condition. We chose individual ZnO NRs as the platform for our investigations due to their easy accessibility via various fabrication methodologies,[16−19] strong SH nonlinear susceptibility,[20] large exciton-binding energy,[21] and confined mode volume.[22] Studies on the nonlinear characteristics of ZnO excitons have been limited, yet recently, Lafrentz et al. demonstrated that ZnO excitons subjected to a magnetic field can act as a source of SHG through the Magneto-stark effect.[23]

Our NR platforms are schematically illustrated in Figure 1a. The left schematic illustrates a bare ZnO NR drop-casted onto an annealed Ag film of 30 ± 5 nm thickness supported by a quartz substrate. In between the quartz and Ag lies a 1 nm thick Ge wetting layer that helps improve the smoothness of the Ag.[24,25] The hybrid NR, shown on the right, is constructed by evaporating an additional 30 ± 5 nm thick layer of Ag onto the bare NR. We focus our studies to incident light polarized parallel (TM-polarized) to the NR axis for two purposes. One

Received: May 25, 2015
Published: August 12, 2015

DOI: 10.1021/acsphotonics.5b00268
ACS Photonics 2015, 2, 1314−1319

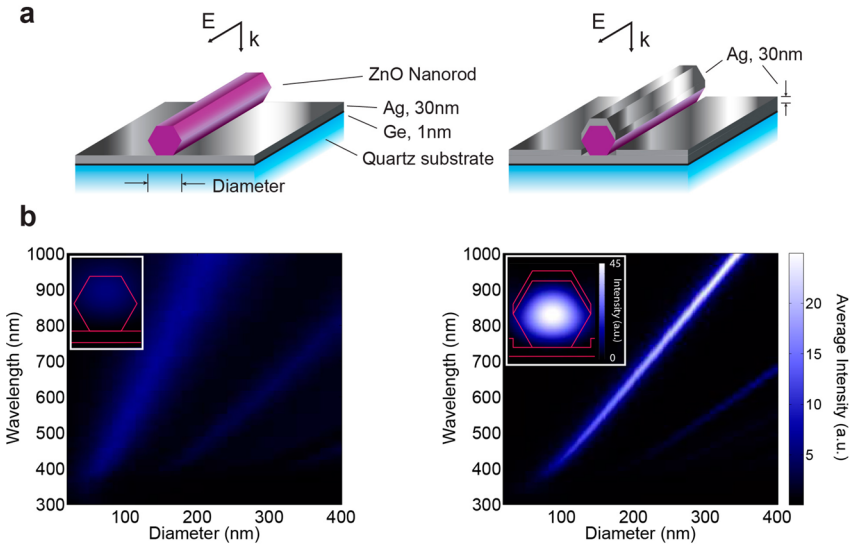

Figure 1. (a) Schematic of a bare (left) and Ag-coated (right) ZnO NR on Ag film. (b) Calculated average intensity within the ZnO NR as a function of wavelength and diameter for a bare (left) and Ag-coated NR (right) on Ag film, generated by TM-polarized light. Insets: Spatial cross sections of the intensity, calculated for diameters of 164 nm (left) and 254 nm (right), each producing maximum intensity at an excitation wavelength of 780 nm.

is to maximize the nonlinear response in line with our original motivation. Of the two susceptibility tensor elements, χ_{zzz} and χ_{zxx}, the component subject to field polarized parallel to the NR axis, χ_{zzz}, is at least twice as large as the component subject to the transverse field, χ_{zxx}.[20] The second purpose is to create a resonance whose field profile provides good spatial overlap with the bulk states.

We illustrate in Figure 1b the average intensity ($|E_{avg}(\lambda,d)|^2$) within the NR as a function of diameter and wavelength. The average intensity is calculated in 2D through a finite difference time domain (FDTD) simulation package (Lumerical, Inc.), where the intensity integrated over the NR core is normalized by the cross-sectional area of the NR core. The average intensity map for the bare NR on Ag film (left panel) reveals resonances apparent as weak bands that are a strong function of diameter and wavelength. These represent Mie solutions[26] occurring below the bandgap, in the regime of negligible but finite loss, also known in the context of nanowires as leaky-mode resonances.[13] When coated with a 30 nm thick Ag coating, the bands display a modified dispersion while exhibiting dramatically increased peaks and narrowed widths (Figure 1b, right panel). We observe that the Ag cavity is able to enhance the resonant mode by concentrating light into the center of the NR several times more efficiently than with a bare NR, as shown in the spatial profiles of the lowest order Mie resonances in the insets of Figure 1b. The strong spatial overlap between field and center of NR facilitates spatial coupling of frequency-doubled light to the bulk excitons. This behavior contrasts with that of plasmonically generated fields that are bound to the metal interface. We present in Figure S1 the mode area normalized by the simulated area for the bare and coated NRs at their respective lowest order Mie resonances as a function of diameter. It is apparent that a hybrid NR of a diameter larger than ∼80 nm results in stronger light−matter interactions than that produced by a bare NR of the same size, as can be observed from the smaller mode area exhibited by the hybrid NR. From the diameter-wavelength dispersion of the lowest order resonant mode (herein, referred to as just cavity resonance), we identified the range of NR diameters required to generate a cavity enhanced SH (FH) signal between 360 (720) and 400 (800) nm, which includes the ZnO exciton wavelength, to be between 220 and 260 nm.

Ultrahigh purity ZnO NRs of wurtzite crystal structure were prepared by using metal−organic vapor-phase epitaxy[18] (MOVPE), with nominal diameters in our target range enabled by controlling the growth duration. Verified by room-temperature PL measurements, the ZnO NRs displayed negligible defects in the visible and near infrared (NIR) due to the absence of metal catalyst particles during growth (see Figure S2).[27] Such characteristics enable an ideally clean system for SHG studies in our wavelength range of interest. From the same measurements, the exciton wavelength was determined to be 379 nm. We note that most NRs displayed some degree of tapering along their length due to the extended growth duration, wherein excessive tapering can lead to decreased intensities and broadened cavity resonance widths. Since the region of least tapering contributes the most to the cavity resonance, the nominal diameter of the NR was defined by this region.

Four NRs with diameters of 219, 236, 243, and 252 ± 9 nm, shown in Figure 2a from top to bottom, respectively, were selected to demonstrate the enhancement and diameter-dependence of the cavity resonances when coated with Ag. We employed a transmission setup described in the Supporting Information and Figure S5, where each hybrid NR was locally excited by a supercontinuum white light laser (Fianium) focused by a 0.4 NA objective lens. Contrary to intuition, we observed a transmission peak instead of a valley at wavelengths corresponding to enhanced absorption, as shown in Figure 2b, where the absorption is due to the finite loss components in the ZnO and can be used to indirectly monitor the field intensity in the NR. An analogous observation of transmission and absorption both exhibiting peaks at similar wavelengths was made in absorbent-filled metallic holes[28] and explained as an absorption-induced reduction in evanescent waves in the holes.[29] In our case, an equivalent interpretation based on cancellation of dipolar scattering in the NR interior by the Ag exterior can be applied,[30] resulting in transparency localized

DOI: 10.1021/acsphotonics.5b00268
ACS Photonics 2015, 2, 1314−1319

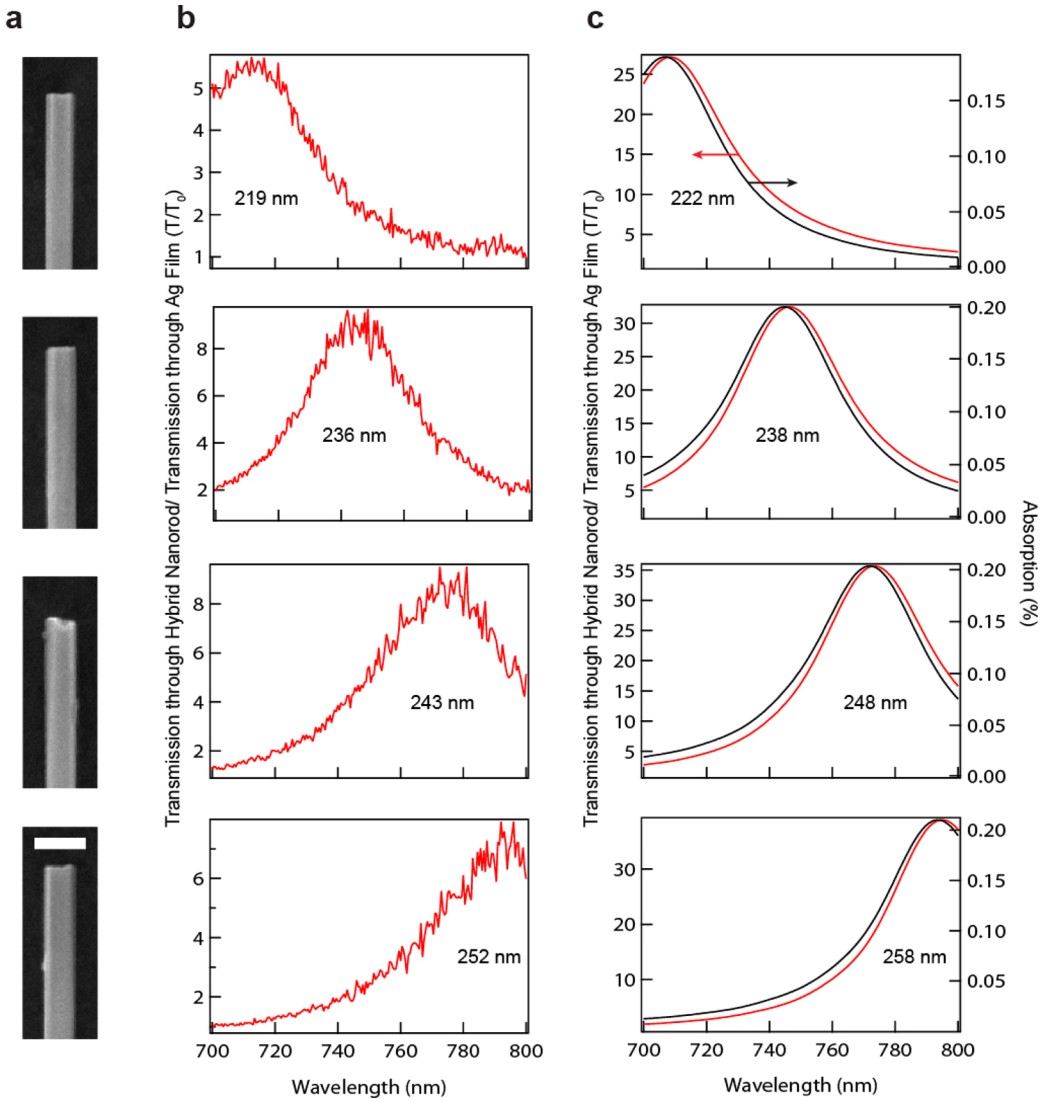

Figure 2. Verifying the tunability of the FH cavity resonances with the hybrid NRs. (a) SEM images of NRs before Ag coating. Nominal diameters from top to bottom are 219, 236, 243, and 252 ± 9 nm, respectively. Scale bar is 400 nm. (b) Transmission through the respective NRs shown in (a) after coated with Ag, normalized by transmission through the neighboring bare region (T/T_0). (c) Calculated T/T_0 (red line) and absorption (black line) for hybrid NRs with diameters of 222, 238, 248, and 258, and a Ag cavity shell thickness of 28 nm.

around the NR. The tunability of the localized transparency was further demonstrated in a separate report on nanoscale visible filters.[31] Figure 2c numerically verifies that the absorption spectrally tracks the normalized transmission, defined as the ratio of transmission through the hybrid NR to that through the Ag background (i.e., T/T_0). This near-equivalence between the transmission and absorption lineshapes allows us to extract the center wavelength, λ_c, and line width of the cavity resonance from the normalized transmission using the relation: $I \sim (T(\omega)/T_0(\omega)/[\omega \mathrm{Im}(\varepsilon(\omega))])$.

The best calculated fit to the experimental transmission was obtained for a Ag layer thickness of 28 nm on NRs with diameters of 222, 238, 248, and 258 nm, respectively, staying well within the error range of the experimental parameters. The quality factors of the resonances measured from each hybrid NR ranged from 11 to 17 compared to the theoretical quality factors of 18 to 21. We note that the normalized transmission peaks from the measurement are 4−5-fold lower than those from the numerical calculations. This discrepancy can be attributed to experimental factors such as the larger beam spot size compared to the Abbe diffraction limit used in the calculations, contributions from tapered regions, and surface roughness of the Ag.

Once the enhancement and tunability of the cavity resonance in the FH were verified, we frequency-doubled the resonances. A tunable Ti:sapphire femtosecond laser (Coherent Inc.) was employed as the pump source in a setup similar to the transmission measurement described above (see Supporting Information and Figure 3a). The excitation was focused with a 0.4 NA objective lens, while the transmission was collected by a 0.5 NA UV objective lens and analyzed by a CCD spectrometer after removing the excitation beam with a short-pass filter. The SHG was monitored from 360 to 400 nm by scanning the pump wavelength of the femtosecond laser from 720 to 800 nm, while power for each wavelength was maintained at 300 μW. No SHG was observed in the bare Ag background or underlying quartz. Since the NR diameters of interest were less than the coherence length of ZnO (>600 nm in the wavelength range from 700 to 900 nm), we assumed complete phase-matching within the plane normal to the NR axis.

DOI: 10.1021/acsphotonics.5b00268
ACS Photonics 2015, 2, 1314−1319

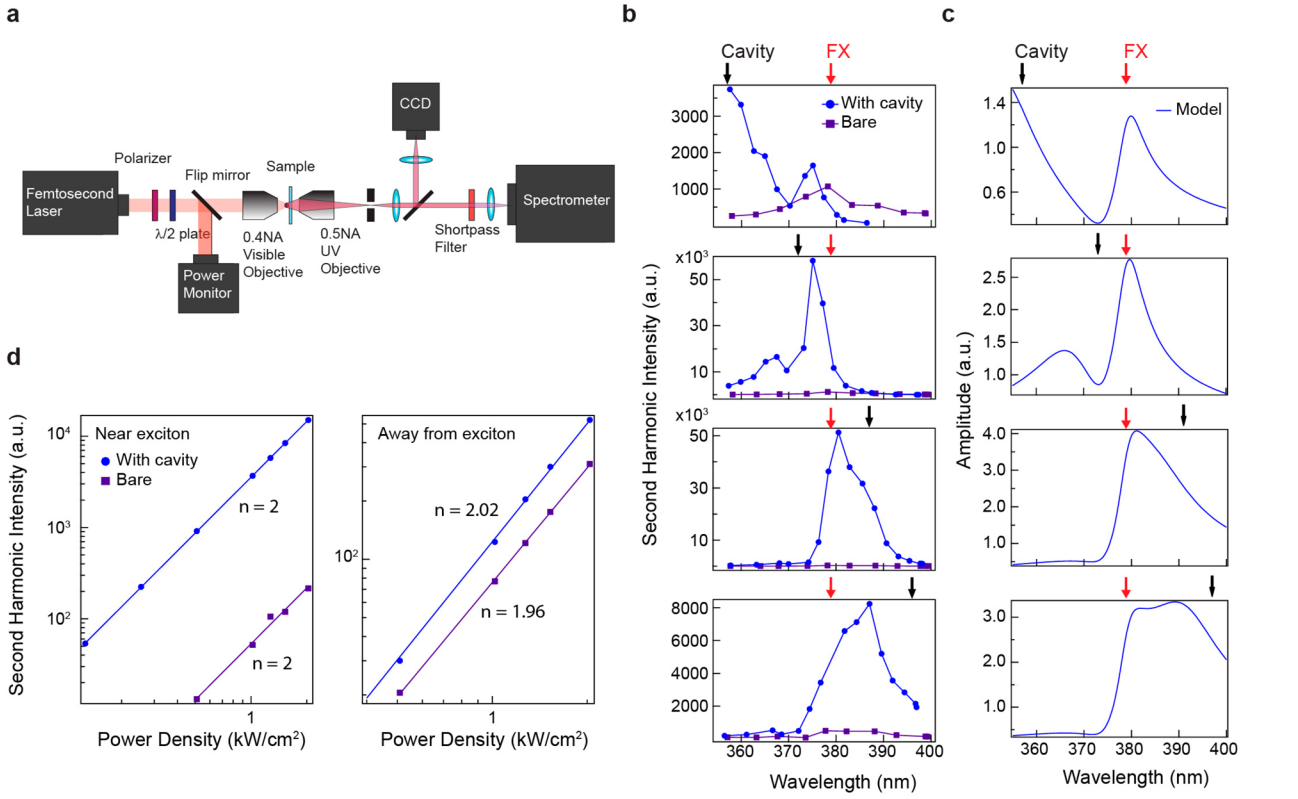

Figure 3. (a) Schematic for measuring SHG in individual NRs. (b) Measured SHG from the hybrid NRs shown in Figure 2, before (purple line) and after (blue line) Ag coating. The black arrow marks the center of the frequency-doubled cavity resonance. The red arrow marks the exciton wavelength. (c) Calculated amplitude from a system of classical harmonic oscillators involving coupling between frequency-doubled cavity resonance and exciton ensemble. The black arrow marks the center of the frequency-doubled cavity resonance. The red arrow marks the exciton wavelength. (d) Second harmonic intensities as a function of power before (purple line) and after (blue line) Ag coating on a NR, measured at wavelengths near (left panel) and away from (right panel) the exciton wavelength.

Mapping the SH intensities from each of the four hybrid NRs over the scan range of interest reveals lineshapes in Figure 3b (blue line) that differ distinctly from the Lorentzian-shaped profiles shown in Figure 2b. For each hybrid NR, we denote the exciton wavelength with a red arrow labeled FX and the center of the cavity resonance shown at its SH wavelength ($\lambda_c/2$) with a black arrow labeled cavity. One noticeable difference compared to the response in the FH is that the center of cavity resonance does not coincide, in general, with wavelength producing maximum SH intensity. In fact, when the black arrow is below the red arrow fixed at 379 nm (see top two panels of Figure 3b), the SH response is split into two peaks, with a pronounced dip fixed near 370 nm. Furthermore, when the black arrow is above the red arrow (see bottom two panels in Figure 3b), the maximum SH response is significantly blue-shifted from the center of cavity resonance while displaying highly asymmetric lineshapes. We attribute these findings to clear signatures of coherent coupling between a collection of free excitons excited by the second harmonic process and frequency-doubled cavity resonance using the following model.

A classical coupled oscillator system (see Supporting Information) was employed to model the coupled response of our hybrid NR. Coupled oscillators have served as a versatile and intuitive model for describing strongly interacting quantum systems,[32] the excitonic response of carbon nanotubes on metamaterials,[9] and electromagnetically induced transparency (EIT).[33] Our model makes a few simplifications to our system to help distill the essential physical process. Since the interplay between the two resonances occurs within the same harmonic order, we treat the cavity and exciton resonances as a linearly coupled system. Due to the large spatial extension of the concentrated field generated by the cavity, as seen in the right inset of Figure 1b, an ensemble of excitons is predicted to be coherently excited. This picture is captured in our model by coupling a large number of exciton oscillators with identical properties to a single cavity resonator (see Figure S7a). For each hybrid NR, the SH process was phenomenologically treated by determining the line width of the frequency-doubled cavity resonator, γ_c, from a Lorentzian fit to the square of the intensity peak, found from Figure 2c, projected to its SH wavelength since $I(2\omega) \sim I^2(\omega)$ (see Figure S7b). Employing this method, we determined γ_c for the four hybrid NRs to be 0.14, 0.13, 0.15, and 0.14 eV from top to bottom panels, respectively. The line width characterizing the excitonic resonance, γ_x, also created by the SH process, was extracted from a Lorentzian fit to the experimentally determined two photon luminescence (TPL) peak, generated by pumping above half the bandgap (see Figure S7c). From this method, the excitonic line width was determined to be 0.05 eV.

Despite its simplicity, the model reproduces the general features of the measured profiles in Figure 3b as the center of the frequency-doubled cavity resonance (black arrow) is scanned across the exciton wavelength (red arrow), as shown in Figure 3c. When the frequency-doubled cavity resonator is tuned above the exciton oscillator wavelength and driven near the exciton oscillator wavelength, the normal modes of the

DOI: 10.1021/acsphotonics.5b00268
ACS Photonics 2015, 2, 1314−1319

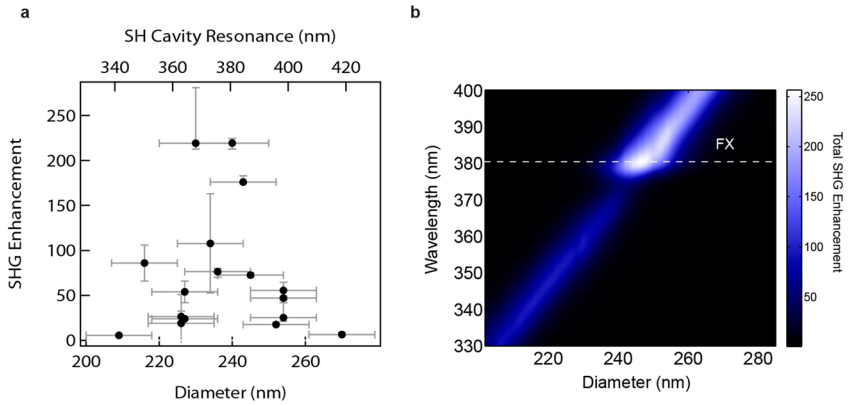

Figure 4. (a) Total SHG enhancement from Ag-coated ZnO NRs on Ag film relative to the case before Ag coating. (b) Predicted total enhancement in SHG due to the enhanced FH field from the Ag cavity and exciton−cavity coupling in the SH as a function of wavelength and diameter.

system undergo constructive interference. When the frequency-doubled cavity resonator is tuned below the exciton oscillator wavelength and driven near 373 nm, below the exciton oscillator wavelength, the normal modes experience destructive interference. This is experimentally observed as the dip near 370 nm. The ∼40 meV discrepancy between model and measurement in absolute position of spectral features may originate from our exclusion of the interaction between excitons or the absence of optical phonons in the model.[34] We remove the possibility of nonlinear coupling between the cavity resonator and excitons because no change in line shape or shift in features was observed in our measurements for increasing pump powers up to 800 μW.

We confirmed that the second harmonic process is maintained, even with the excitonic coupling, by measuring the SH intensity as a function of power and extracting the slope from its log−log plot (see Figure 3d) in a hybrid NR whose frequency-doubled cavity resonance falls near the exciton wavelength. The SHG-power dependence was measured at wavelengths near and away from the exciton wavelength, each before and after Ag coating. For SH wavelengths near the exciton wavelength, pump wavelengths of 755 and 760 nm were used for the hybrid and bare NR, respectively, while for SH wavelengths away from the exciton wavelength, pump wavelengths of 780 and 800 nm were used, respectively. Figure 3d shows that the slope from the log−log plot is consistently ∼2 for SH wavelengths that are both close and distant to the excitonic transition before and after the Ag coating. This indicates that, although the exciton coupling enhances the SHG, it does not fundamentally alter the SH process.

In order to quantify the enhancement in UV brightness due to the combined effects of enhanced FH resonance and exciton−cavity coupling in the SH, we measured the SHG enhancements of Ag-coated NRs relative to the case before the Ag-coating. Displayed as purple curves in Figure 3b, the SH response from each bare NR was obtained from the same hybrid NR prior to the Ag-coating. As expected from the weak intensity bands shown in the left panel of Figure 1b, the SH responses do not show any pronounced features. Figure 4a presents the experimentally obtained SHG enhancements. Maximum SHG enhancements near 200-fold were achieved in 230−240 nm diameter NRs, corresponding to frequency-doubled cavity resonances close to the exciton wavelength.

Total SHG enhancements can be predicted from the product, $(I_{\text{hybrid}}(2\omega)/I_{\text{bare}}(2\omega))\cdot(I_{\text{FX-hybrid}}(2\omega)/I_{\text{hybrid}}(2\omega))$, where $I_{\text{hybrid}}(2\omega)$ and $I_{\text{FX-hybrid}}(2\omega)$ represent the SH intensity from a hybrid NR, excluding and including excitonic coupling, respectively, while $I_{\text{bare}}(2\omega)$ represents the SHG from a bare NR. The first factor provides the SHG enhancement due to the Ag-cavity induced FH field enhancement, while the second expresses that due to coupling between enhanced field and free excitons both excited in the SH. Since $I_{\text{SHG}}(2\omega) \sim (\chi_{zzz}|E_z(\omega)|^2)^2$, we calculate the first enhancement factor as $|E_{\text{hybrid}}(\omega)|^4/|E_{\text{bare}}(\omega)|^4$ using the FH fields extracted from FDTD simulations, yielding enhancements near the exciton wavelength close to 80-fold (see Figure S9a). The second factor is obtained from our oscillator model by finding the ratio between the field amplitude with and without excitonic coupling. When the frequency-doubled cavity resonance is close to the exciton wavelength, enhancement is maximized by 3-fold (see Figure S9b). We note that higher enhancements are achievable using smaller exciton resonance line widths, which can be experimentally realized by improving the material quality. The product of the two enhancement factors results in a maximum enhancement near 250-fold for NR diameters producing frequency-doubled cavity resonances close to the exciton wavelength as shown in Figure 4b, consistent with our experimental observations.

In summary, we have enhanced the SHG from a ZnO NR by first increasing it with a Ag-cavity via enhanced field in the FH and then by modifying the frequency-doubled field through coherent coupling to an ensemble of free excitons in the SH. While the lowest-order Mie resonance enabled good spatial overlap, spectral overlap was achieved by tuning the frequency-doubled resonance toward the exciton wavelength through the NR diameter, resulting in large and coherent light−matter interaction. The accessibility of the hybrid structure can be appreciated from the fact that the Ag cavity, critical in generating the observed phenomena, can be constructed by two sequential blanket coatings of Ag before and after the placement of the NR. In a size regime that represents an elusive frontier for plasmonic enhancements, the aforementioned aspects highlight a general and simple avenue for effectively increasing the nonlinear responses of noncentrosymmetric systems orders of magnitude beyond their intrinsic limits.

■ ASSOCIATED CONTENT

Supporting Information

The Supporting Information is available free of charge on the ACS Publications website at DOI: 10.1021/acsphotonics.5b00268.

DOI: 10.1021/acsphotonics.5b00268
ACS Photonics 2015, 2, 1314−1319

Details on mode area, sample fabrication, transmission measurement, nonlinear femtosecond measurement, numerical simulation, comparisons to an ideal core−shell nanowire, analytical model for coupled exciton-cavity resonance, verification for involvement of ensemble of excitons, and individual enhancement factors (PDF)

AUTHOR INFORMATION

Corresponding Author

*E-mail: gcyi@snu.ac.kr.

Notes

The authors declare no competing financial interest.

ACKNOWLEDGMENTS

This work was financially supported by Future-Based Technology Development Program (Nano Fields) through the National Research Foundation (NRF) of Korea, funded by the Ministry of Education, Science and Technology (MEST; No. 2014M3A7B4051589), and the SNU-Yonsei Research Cooperation Program through Seoul National University (SNU) in 2014. T.K. and D.K. acknowledge the support by the National Research Foundation of Korea (NRF) grant funded by the Korea government (MSIP; No. 2008-0061906, 2005-0093838, 2008-00580) and the Brain Korea 21 Plus Project in 2014. J.K.H. acknowledges support from the TJ Park Science Fellowship through the POSCO TJ Park Foundation and the Ewha Womans University Research Grant of 2015.

REFERENCES

(1) Sorger, V. J.; Oulton, R. F.; Ma, R. M.; Zhang, X. Toward integrated plasmonic circuits. *MRS Bull.* **2012**, *37*, 728−738.

(2) Nakayama, Y.; Pauzauskie, P. J.; Radenovic, A.; Onorato, R. M.; Saykally, R. J.; Liphardt, J.; Yang, P. D. Tunable nanowire nonlinear optical probe. *Nature* **2007**, *447*, 1098−U8.

(3) Achermann, M. Exciton-Plasmon Interactions in Metal-Semiconductor Nanostructures. *J. Phys. Chem. Lett.* **2010**, *1*, 2837−2843.

(4) Vasa, P.; Pomraenke, R.; Schwieger, S.; Mazur, Y. I.; Kunets, V.; Srinivasan, P.; Johnson, E.; Kihm, J. E.; Kim, D. S.; Runge, E.; Salamo, G.; Lienau, C. Coherent exciton-surface-plasmon-polariton interaction in hybrid metal-semiconductor nanostructures. *Phys. Rev. Lett.* **2008**, *101*, 116801.

(5) Govorov, A. O.; Bryant, G. W.; Zhang, W.; Skeini, T.; Lee, J.; Kotov, N. A.; Slocik, J. M.; Naik, R. R. Exciton-plasmon interaction and hybrid excitons in semiconductor-metal nanoparticle assemblies. *Nano Lett.* **2006**, *6*, 984−994.

(6) Zhang, J. T.; Tang, Y.; Lee, K.; Ouyang, M. Tailoring light-matter-spin interactions in colloidal hetero-nanostructures. *Nature* **2010**, *466*, 91−95.

(7) Pu, Y.; Grange, R.; Hsieh, C. L.; Psaltis, D. Nonlinear Optical Properties of Core-Shell Nanocavities for Enhanced Second-Harmonic Generation. *Phys. Rev. Lett.* **2010**, *104*, 207402.

(8) Kauranen, M.; Zayats, A. V. Nonlinear plasmonics. *Nat. Photonics* **2012**, *6*, 737−748.

(9) Nikolaenko, A. E.; De Angelis, F.; Boden, S. A.; Papasimakis, N.; Ashburn, P.; Di Fabrizio, E.; Zheludev, N. I. Carbon Nanotubes in a Photonic Metamaterial. *Phys. Rev. Lett.* **2010**, *104*, 153902.

(10) Lee, J.; Govorov, A. O.; Dulka, J.; Kotov, N. A. Bioconjugates of CdTe nanowires and Au nanoparticles: Plasmon-exciton interactions, luminescence enhancement, and collective effects. *Nano Lett.* **2004**, *4*, 2323−2330.

(11) Cho, C. H.; Aspetti, C. O.; Turk, M. E.; Kikkawa, J. M.; Nam, S. W.; Agarwal, R. Tailoring hot-exciton emission and lifetimes in semiconducting nanowires via whispering-gallery nanocavity plasmons. *Nat. Mater.* **2011**, *10*, 669−675.

(12) Hyun, J. K.; Lauhon, L. J. Spatially Resolved Plasmonically Enhanced Photocurrent from Au Nanoparticles on a Si Nanowire. *Nano Lett.* **2011**, *11*, 2731−2734.

(13) Cao, L. Y.; White, J. S.; Park, J. S.; Schuller, J. A.; Clemens, B. M.; Brongersma, M. L. Engineering light absorption in semiconductor nanowire devices. *Nat. Mater.* **2009**, *8*, 643−647.

(14) Grinblat, G.; Rahmani, M.; Cortes, E.; Caldarola, M.; Comedi, D.; Maier, S. A.; Bragas, A. V. High-Efficiency Second Harmonic Generation from a Single Hybrid ZnO Nanowire/Au Plasmonic Nano-Oligomer. *Nano Lett.* **2014**, *14*, 6660−6665.

(15) Ren, M. L.; Liu, W. J.; Aspetti, C. O.; Sun, L. X.; Agarwal, R. Enhanced second-harmonic generation from metal-integrated semiconductor nanowires via highly confined whispering gallery modes. *Nat. Commun.* **2014**, *5*, 5432.

(16) Yi, G. C.; Wang, C. R.; Park, W. I. ZnO nanorods: synthesis, characterization and applications. *Semicond. Sci. Technol.* **2005**, *20*, S22−S34.

(17) Vayssieres, L. Growth of arrayed nanorods and nanowires of ZnO from aqueous solutions. *Adv. Mater.* **2003**, *15*, 464−466.

(18) Park, W. I.; Kim, D. H.; Jung, S. W.; Yi, G. C. Metalorganic vapor-phase epitaxial growth of vertically well-aligned ZnO nanorods. *Appl. Phys. Lett.* **2002**, *80*, 4232−4234.

(19) Kong, Y. C.; Yu, D. P.; Zhang, B.; Fang, W.; Feng, S. Q. Ultraviolet-emitting ZnO nanowires synthesized by a physical vapor deposition approach. *Appl. Phys. Lett.* **2001**, *78*, 407−409.

(20) Johnson, J. C.; Yan, H. Q.; Schaller, R. D.; Petersen, P. B.; Yang, P. D.; Saykally, R. J. Near-field imaging of nonlinear optical mixing in single zinc oxide nanowires. *Nano Lett.* **2002**, *2*, 279−283.

(21) Djurisic, A. B.; Leung, Y. H. Optical properties of ZnO nanostructures. *Small* **2006**, *2*, 944−961.

(22) van Vugt, L. K.; Ruhle, S.; Ravindran, P.; Gerritsen, H. C.; Kuipers, L.; Vanmaekelbergh, D. Exciton polaritons confined in a ZnO nanowire cavity. *Phys. Rev. Lett.* **2006**, *97*, 147401.

(23) Lafrentz, M.; Brunne, D.; Kaminski, B.; Pavlov, V. V.; Rodina, A. V.; Pisarev, R. V.; Yakovlev, D. R.; Bakin, A.; Bayer, M. Magneto-Stark Effect of Excitons as the Origin of Second Harmonic Generation in ZnO. *Phys. Rev. Lett.* **2013**, *110*, 116402.

(24) Chen, W.; Chen, K. P.; Thoreson, M. D.; Kildishev, A. V.; Shalaev, V. M. Ultrathin, ultrasmooth, and low-loss silver films via wetting and annealing. *Appl. Phys. Lett.* **2010**, *97*, 211107.

(25) Vj, L.; Kobayashi, N. P.; Islam, M. S.; Wu, W.; Chaturvedi, P.; Fang, N. X.; Wang, S. Y.; Williams, R. S. Ultrasmooth Silver Thin Films Deposited with a Germanium Nucleation Layer. *Nano Lett.* **2009**, *9*, 178−182.

(26) Bohren, C. F.; Huffman, D. R. *Absorption and Scattering of Light by Small Particles*; Wiley-VCH: New York, 1983.

(27) Park, W. I.; Jun, Y. H.; Jung, S. W.; Yi, G. C. Excitonic emissions observed in ZnO single crystal nanorods. *Appl. Phys. Lett.* **2003**, *82*, 964−966.

(28) Hutchison, J. A.; O'Carroll, D. M.; Schwartz, T.; Genet, C.; Ebbesen, T. W. Absorption-Induced Transparency. *Angew. Chem., Int. Ed.* **2011**, *50*, 2085−2089.

(29) Rodrigo, S. G.; Garcia-Vidal, F. J.; Martin-Moreno, L. Theory of absorption-induced transparency. *Phys. Rev. B: Condens. Matter Mater. Phys.* **2013**, *88*, 155126.

(30) Alu, A.; Engheta, N. Achieving transparency with plasmonic and metamaterial coatings. *Phys. Rev. E* **2005**, *72*, 016623.

(31) Hyun, J. K.; Kang, T.; Baek, H. J.; Jeon, S.; Kim, D. S.; Yi, G. C. Nanoscale Single-Element Color Filters. *Nano Lett.* **2015**, DOI: 10.1021/acs.nanolett.5b02049.

(32) Novotny, L. Strong coupling, energy splitting, and level crossings: A classical perspective. *Am. J. Phys.* **2010**, *78*, 1199−1202.

(33) Alzar, C. L. G.; Martinez, M. A. G.; Nussenzveig, P. Classical analog of electromagnetically induced transparency. *Am. J. Phys.* **2002**, *70*, 37−41.

(34) Capeluto, M. G.; Grinblat, G.; Tirado, M.; Comedi, D.; Bragas, A. V. Nonlinear excitation of polariton cavity modes in ZnO single nanocombs. *Opt. Express* **2014**, *22*, 5341−5349.

DOI: 10.1021/acsphotonics.5b00268
ACS Photonics 2015, 2, 1314−1319